

# Hardware and GNC solutions for controlled spacecraft re-entry using aerodynamic drag



Sanny R. Omar\*, Riccardo Bevilacqua

Department of Mechanical and Aerospace Engineering, University of Florida, 939 Sweetwater Dr., Gainesville, FL, 32611, USA

## ARTICLE INFO

### Keywords:

Controlled Re-Entry  
CubeSat  
Guidance generation  
Feedback control  
Aerodynamic drag

## ABSTRACT

Traditionally, controlled spacecraft re-entries have been conducted using propulsive de-orbit burns which are risky, expensive, and may not be possible for all vehicles. Recently, the miniaturization of technology has ushered in a new class of small satellites (such as CubeSats) that are too small to host thrusters but may require a controlled de-orbit if they contain materials capable of surviving re-entry. For all space vehicles requiring a controlled re-entry, the ability to harness the naturally occurring aerodynamic drag force for orbit control provides a cheaper and more reliable alternative to chemical propulsion.

This paper discusses a comprehensive method for drag-controlled re-entry that is applicable to any vehicle capable of modulating its ballistic coefficient. First, a novel guidance generation algorithm efficient enough to run onboard a CubeSat outputs a desired ballistic coefficient profile and corresponding numerically propagated trajectory that if followed, will lead the spacecraft to a desired de-orbit location. This guidance generation algorithm is based on an analytical solution that provides convergence guarantees, ensures rapid performance, and facilitates a controllability analysis. Next, the guidance tracking algorithm utilizes an extended Kalman filter and GPS measurements to estimate the position and velocity of the satellite relative to the guidance. A full state feedback linear-quadratic-regulator (LQR) control strategy is then used to drive the relative position and velocity to zero using solely aerodynamic drag. This paper also discusses a novel retractable drag de-orbit device (D3) that can be attached to existing CubeSat structures and can easily be scaled up for larger satellites. The D3 provides passive three-axis attitude stabilization using aerodynamic and gravity gradient forces and can be repeatedly modulated to perform aerodynamically-based orbital maneuvering and controlled re-entry. The design of the planned 2U CubeSat to test the D3 and control algorithms in flight is also discussed.

The re-entry point targeting algorithms were validated through extensive Monte Carlo simulations which included realistic GPS measurement errors and drag force uncertainties. The algorithms were able to guide the satellite to a desired de-orbit location with an average error below 25 km and in all cases, the targeting error was low enough for debris mitigation purposes. The accuracy and reliability of these algorithms coupled with the D3 device that has successfully undergone thermal vacuum, vibration, and fatigue testing provide a cheap, reliable, and comprehensive attitude, orbit, and de-orbit control solution that can be used on large and small space vehicles, possibly replacing conventional propulsion and attitude control systems and making space more accessible to everyone.

## 1. Introduction

The increasing number of space vehicles launched has led to an increasing concern with orbital debris mitigation [1]. NASA requirements [2] state that low Earth orbit (LEO) spacecraft must de-orbit within 25 years and that the probability of human casualty from re-entering debris must be less than 1 in 10,000. Aerodynamic drag presents itself as a convenient and efficient way to expedite de-orbit and control the re-entry location of a LEO spacecraft without using

thrusters. While several teams have developed drag devices and tested them in orbit [3–5], the majority of these devices have been single-use drag sails that cannot be retracted. These devices had been developed with the sole purpose of expediting the de-orbit of a host satellite. The PADDLES retractable drag sail was developed previously by the University of Florida ADAMUS lab to facilitate orbital maneuvering [6], but has not yet flown. The ExoBrake drag device [7,8] developed by NASA Ames deploys in a parachute shape and can be partially retracted, but is limited by how far it can retract and how many deploy-retract cycles it

\* Corresponding author.

E-mail addresses: [sanny.omar@gmail.com](mailto:sanny.omar@gmail.com) (S.R. Omar), [bevilr@ufl.edu](mailto:bevilr@ufl.edu) (R. Bevilacqua).

<https://doi.org/10.1016/j.actaastro.2019.03.051>

Received 6 January 2019; Received in revised form 22 February 2019; Accepted 16 March 2019

Available online 21 March 2019

0094-5765/ © 2019 IAA. Published by Elsevier Ltd. All rights reserved.

**Nomenclature**

$a$	semi major axis
$C_b$	ballistic coefficient
$e$	eccentricity
$I$	identity matrix
$i$	inclination
$J_2$	gravitational perturbation due to Earth's oblateness
$R_e$	Earth's equatorial radius
$t$	time
$u$	argument of latitude
$\mathbf{v}$	velocity vector
$\Omega$	right ascension of ascending node
$\mu$	Earth's gravitational parameter

**Acronyms/Abbreviations**

D3	Drag De-Orbit Device
EKF	Extended Kalman Filter
GPS	Global Positioning System
GRMS	Root-Mean-Square Acceleration
ISS	International Space Station
LQR	Linear Quadratic Regulator
LEO	Low Earth Orbit
LVLH	Local Vertical Local Horizontal
PPOD	Poly-Picosatellite Orbital Deployer
TRL	Technology Readiness Level

can perform. The ExoBrake is thus far the only drag device launched that can be utilized to perform orbital maneuvering [8], but successful maneuvering with the ExoBrake has not been demonstrated so far and the controlled re-entry algorithms developed by that team involve up-linking a pre-computed set of desired ballistic coefficients to the satellite and applying these open loop [9]. In addition, while the ExoBrake provides passive aerodynamic stability if it is deployed while in the correct orientation, the ExoBrake is incapable of constraining rotation about the roll axis [8]. While multiple algorithms for orbital maneuvering using aerodynamic drag exist [10–13] and Planet Labs has a CubeSat constellation with separation controlled by differential drag [14], to date there has not been a successful controlled de-orbit of a spacecraft using entirely aerodynamic drag.

The University of Florida ADAMUS lab, with funding from the NASA Launch Services Program (LSP) and Florida Space Research Initiative (SRI), has developed a new retractable drag de-orbit device (D3) capable of modulating the drag area of a host CubeSat while maintaining passive 3-axis attitude stabilization using aerodynamic and gravity gradient torques [15]. The D3 can be utilized for orbital maneuvering, reduction of orbit lifetime, collision avoidance, and targeted re-entry. The D3 is not designed to survive re-entry and is intended to guide the host satellite to a desired de-orbit point (likely over the ocean) such that any debris surviving re-entry will not pose a hazard to ground assets. The goal of the D3 is to provide an affordable yet reliable and easy to integrate device that will enable LEO CubeSats to meet or exceed NASA debris mitigation requirements and will facilitate advanced CubeSat missions through enhanced attitude and orbit control. Satellite operators wishing to recover orbital payloads (possibly for ISS sample return missions) could use the D3 to guide their spacecraft to a re-entry point but would need a heat shield and a secondary control apparatus to protect and guide the payload through re-entry. As a part of the project, a targeted re-entry algorithm has been developed that determines how the D3 should modulate its deployment level to re-enter the spacecraft in a desired location [16]. This algorithm offers improvements in robustness and reliability over the state of the art and is efficient enough to run onboard a CubeSat with a high-performance processor such as a BeagleBone Black or Xiphos Q7. Feedback Control techniques are employed to ensure that the spacecraft follows a desired trajectory to the de-orbit point [16]. While the re-entry point targeting algorithm was developed with the D3 in mind, the algorithm can be utilized on any spacecraft capable of modifying its ballistic coefficient and precisely measuring its position and velocity. Once the technique is validated, large vehicles such as rocket upper stages can achieve drag modulation through attitude changes or the use of a drag device and utilize the targeting algorithm to control their re-entry locations and minimize the risk associated with re-entry debris. Presently, upper stages use residual propellant to perform a controlled de-orbit burn, so the ability to harness the naturally occurring aerodynamic drag for this purpose would eliminate the need for a propulsive de-orbit burn, saving fuel and

ultimately enabling the launch vehicle to carry a larger payload. The enhanced payload capacity could easily translate to millions of dollars of savings. The targeting algorithm could also be utilized to facilitate the landings of probes on other planets with atmospheres without the need for thrusters.

This paper first gives an overview of the D3 device in Section 2. Next, the targeted re-entry algorithms and their expected performances are discussed in Section 3. Section 4 details the planned spacecraft components, Section 5 discusses ground operations, and Section 6 presents power, link, thermal, and vibration analyses. Finally, Section 7 discusses the software development plan and Section 8 discusses the mission concept of operations, presents the mission success criteria, and provides a failure analysis and risk mitigation plan.

## 2. Drag de-orbit device (D3) overview

The drag de-orbit device (or D3) consists of four retractable tape-spring booms inclined at 20° relative to the face of the satellite to which the D3 is attached (x-y plane) as shown in Fig. 1. A zoomed in view of the D3 device and an expanded view of one of the D3 deployers are shown in Fig. 2 and Fig. 3, respectively. The complete design of the D3

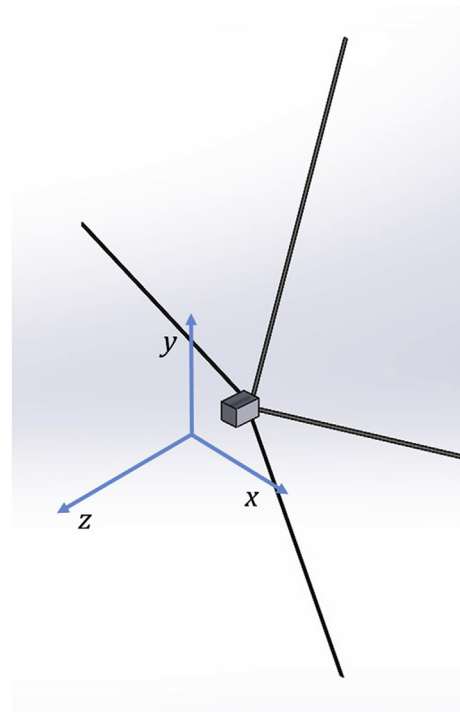


Fig. 1. D3 device attached to a CubeSat with body axes shown.

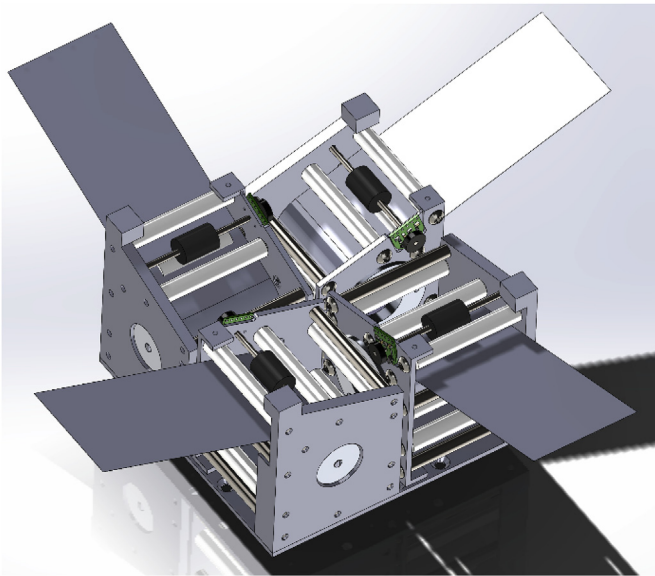


Fig. 2. Zoomed-in view of D3 device.

and the simulations utilized to inform this design are detailed by Guglielmo *et al* [15]. In summary, the “dart” configuration of the D3 booms allows the host satellite to aerodynamically stabilize such that the satellite z-axis (Fig. 1) is aligned with the velocity vector. After multiple simulations with varying booms angles, a 20° angle was selected because shallower boom angles significantly degraded the attitude stability without providing a significant increase in the drag area while the enhanced attitude stability associated with steeper boom angles was not necessary and the steeper angles resulted in unnecessary reductions of the drag area. The booms are fabricated from pre-cut 4 by 370 cm strips of Austenitic 316 stainless steel shim stock that is 0.0762 mm (.003 inches) thick. Each strip weighs about 95 g. The steel strips are run through a series of dies that place bends in the booms and give them measuring-tape-like shapes. The curved shapes give the booms stiffness and ensure that they will remain rigid despite the expected dynamic, aerodynamic, and thermal bending effects they will experience in space. Additionally, because Austenitic 316 stainless steel is almost completely non-ferromagnetic, the booms will not become magnetized by the Earth's magnetic field and will not impart a destabilizing magnetic hysteresis torque on the spacecraft. Because the booms are 3.7 m long and about 4 cm wide, significant aerodynamic torques are created, facilitating aerodynamic stability up to an altitude

of 700 km. The length of the booms and the ability to actuate each boom independently also allows two booms opposite each other to be partially retracted to create a clear minimum moment of inertia axis along the two deployed booms.

Gravity gradient torques will work to passively align this minimum moment of inertia axis with the nadir vector. The combined effects of gravity gradient and aerodynamic torques enable the D3 to provide passive 3-axis attitude stabilization. To increase the attitude stability, three orthogonal magnetorquers are integrated into the D3 structural interface adapter and serve to damp any attitude oscillations when set to run the B-Dot de-tumble algorithm discussed by Guglielmo *et al* [15]. In the previous design, four stepper motors located inside the deployers were utilized to deploy and retract the booms. Unfortunately, there was not a reliable mapping between motor rotation and boom deployment. The booms would often wind up internally as the motor spun before deploying in spurts and jumps. To facilitate accurate boom deployment, the stepper motors were replaced with brushed DC motors (Faulhaber 1516-006SR with 262:1 spur gearbox) and a rotary encoder (Pololu 12CPR) was integrated into each deployer. As each boom deploys, it drives a silicon wheel on a steel shaft that is attached to the encoder. In this manner, the encoder provides an accurate measurement of the movement of the boom itself. A spring roller is also included to push against the boom and ensure that it remains in contact with the silicon wheel. Prototype (Fig. 4) testing showed that with this new design, the boom would consistently deploy or retract to within about 2 cm of the commanded amount. Additionally, the brushed motors consumed significantly less power than the original stepper motors. Based on prototype testing, each motor required 1 Watt when deploying the boom and pulled a maximum of 4.1 Watts when stalled assuming a fully charged battery voltage of 8.2 V. This puts the nominal power usage for the entire D3 system at 4 W (assuming simultaneous boom operation) and the absolute maximum power consumption if all motors are stalled at 16.4 W. Even 16.4 W is well within the capability of most commercial CubeSat power systems, but in practice, there should never be a situation where all four motors are stalled and require this amount of power. Each deployer, including a fully coiled boom, weighs around 250 g and the prototype of the entire D3 device, including four deployers (with booms), the baseplate, the structural interface adapter, magnetorquer brackets, and magnetorquers weighed 1180 g.

When fully extended, the D3 increases the cross-wind surface area of the host satellite by approximately .5 m<sup>2</sup> enabling a 12U, 15 kg CubeSat to de-orbit from a 700 km circular orbit in 25 years under standard atmospheric conditions. Unlike most other drag devices that can only be deployed once to increase the drag area, the D3 can be repeatedly retracted, facilitating orbital maneuvering, collision avoidance, and re-entry point targeting using aerodynamic drag. A prototype

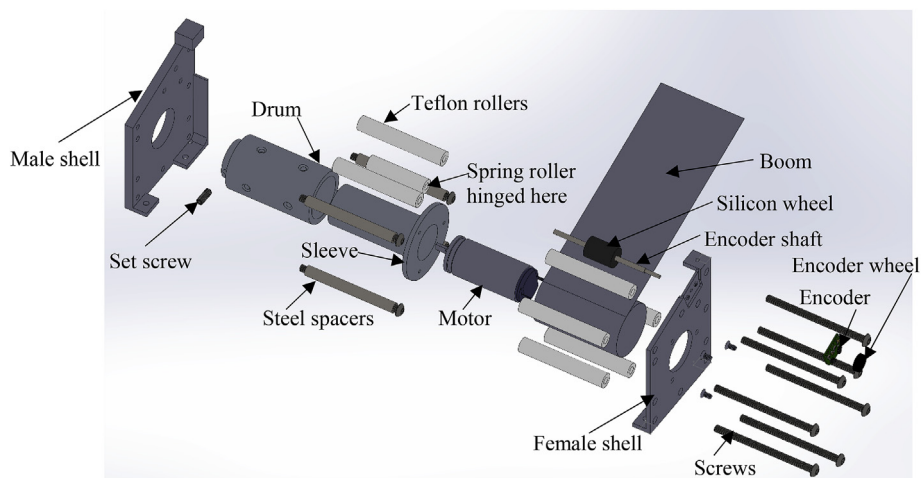


Fig. 3. D3 device deployer expanded view.

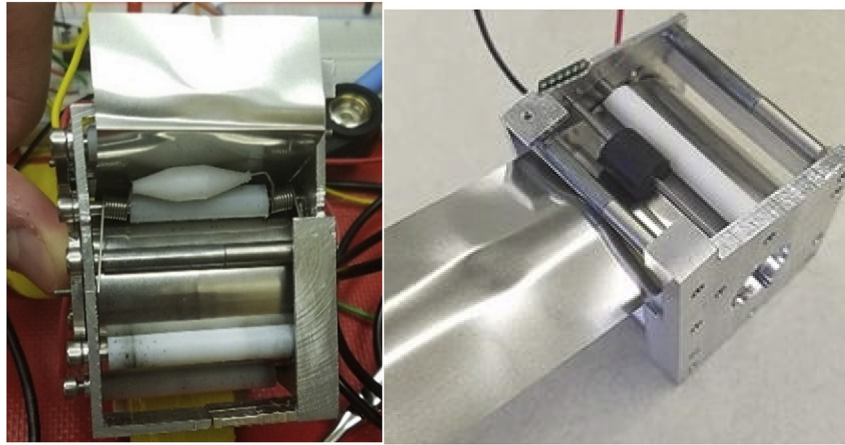


Fig. 4. Prototype of D3 deployer.

of a D3 deployer has also been fatigue tested and functioned nominally after 500 full deploy/retract cycles (more than would be required on an average mission) and continued to operate properly after thermal vacuum testing conducted to simulate the space environment. Multiple shortened deploy/retracted cycles were conducted in the vacuum chamber to simulate a deployer operation equivalent to 10 full length deploy/retract cycles. Future testing plans involve a more rigorous fatigue test of the entire D3 device in vacuum. Vibration testing of a D3 deployer to 9.6 GRMS was also conducted. In this test, a D3 prototype was integrated into a 2U-sized CubeSat structure and the entire assembly was integrated into a PPOD CubeSat deployer prior to vibration to most accurately simulate a launch environment. Functional testing showed all D3 components to be operational and non-damaged after vibration testing. Loctite applied to the D3 screws prevented the loosening of D3 components during vibration.

### 3. Re-entry point targeting algorithm

The purpose of the D3 CubeSat mission is to demonstrate the ability to re-enter the atmosphere in a desired location by varying the spacecraft's aerodynamic drag through modulation of the D3 booms. The drag modulation scheme necessary to de-orbit in the desired location was developed by Omar and Bevilacqua [16] and offers significant improvements over the state of the art [9,17]. The first step in the drag-based re-entry scheme is the guidance generation algorithm. This technique calculates the drag profile that a spacecraft must follow to de-orbit in a desired location. While algorithms in previous literature achieve this using black-box numerical optimizers, the algorithm developed by this author in Ref. [16] utilizes an analytical solution to estimate the necessary drag profile and iteratively refines this estimate via numerical orbit propagation and additional analytical adjustments. The use of the analytical solution in the guidance computation offers convergence guarantees and computational efficiency not available with the algorithms in prior literature. The final guidance returned by the algorithm is a trajectory simulated using the highest fidelity orbit propagator available. If the orbit propagator were a completely accurate reflection of reality, the spacecraft would de-orbit in the desired location if the prescribed boom deployment profile were applied. Unfortunately, even the best models are not perfect and there is significant uncertainty in the drag force prediction. For this reason, a guidance tracking algorithm [16] is utilized that varies the spacecraft's ballistic coefficient using an LQR-based full state feedback control methodology based on the linearized motion of the spacecraft relative to the guidance. An Extended Kalman Filter is utilized to remove sensor noise from the GPS derived relative position and velocity estimates. Prior literature does not heavily investigate guidance tracking or noise filtering as they pertain to this problem. The details of these algorithms

and the means by which they were tested are described below.

#### 3.1. Guidance generation algorithm

The guidance generation algorithm utilizes an analytical solution to estimate the drag profile required to de-orbit in a desired location. This drag profile is simulated using numerical orbit propagation techniques and is continuously refined using analytical techniques and re-simulated based on the discrepancy between the actual and desired de-orbit location. Ultimately, a numerically propagated trajectory and corresponding drag profile are obtained that if followed, will lead the satellite to the desired de-orbit location. The fundamental theory and development of the guidance generation algorithm are discussed in Refs. [16,18]. This section will provide an overview of the algorithm but will focus most heavily on the recent upgrades.

Define the spacecraft ballistic coefficient as

$$C_b = \frac{C_d A}{2m} \quad (1)$$

where  $C_d$  is the drag coefficient,  $A$  is a reference area, and  $m$  is the spacecraft mass. The acceleration due to aerodynamic drag ( $\mathbf{a}_d$ ) acting on the spacecraft is

$$\mathbf{a}_d = -C_b \rho v_\infty \mathbf{v}_\infty \quad (2)$$

where  $\rho$  is the ambient atmospheric density and  $\mathbf{v}_\infty$  is the spacecraft velocity vector relative to the free stream. It is shown in Ref. [16] that given the ability to vary an initial  $C_{b1}$ , a second ballistic coefficient  $C_{b2}$ , and the time  $t_{swap}$  at which the ballistic coefficient is changed from  $C_{b1}$  to  $C_{b2}$ , it is possible to target any point on the Earth with latitude below the orbit inclination if maneuvering is initiated early enough. We will define  $(C_{b1}, C_{b2}, t_{swap})$  as the control parameters. Note that  $C_{b2}$  is maintained until some terminal semi-major axis at which point some pre-set  $C_{bterm}$  is maintained until de-orbit.

The basis of the analytical solution for determining the control parameters needed for proper targeting is the ability to calculate the effect that a perturbation in the control parameters will have on a given trajectory. While a satellite in an unperturbed two-body orbit (spherical Earth) will experience a constant semi-major axis, a satellite in a two-body orbit with drag will experience a monotonically decreasing semi major axis over time. It can be shown [16] that in a circular orbit around a spherical Earth, if a constant, invariant density is assumed at each altitude, then the time and argument of latitude (true anomaly plus argument of perigee) required for a spacecraft to decay from an initial to final semi major axis due to aerodynamic drag increase linearly with decreasing ballistic coefficient. Assume a satellite with ballistic coefficient  $C_{b1}$  takes time  $\Delta t_1$  to achieve some drag-induced change in semi major axis  $\Delta a$  and undergoes argument of latitude change  $\Delta \lambda_1$

while achieving this  $\Delta a$ . The time and argument of latitude change a satellite with the same initial conditions and some different  $C_{b2}$  will undergo to achieve the same  $\Delta a$  (same orbital decay) are given by

$$\Delta t_2 = \frac{C_{b1} \Delta t_1}{C_{b2}} \quad (3)$$

$$\Delta u_2 = \frac{C_{b1} \Delta u_1}{C_{b2}} \quad (4)$$

Since the average rate of change of right ascension ( $\dot{\Omega}_{avg}$ ) is independent of  $C_b$ , the change in  $\Omega$  experienced during the orbital decay can be calculated by

$$\Delta \Omega = \dot{\Omega}_{avg} \Delta t \quad (5)$$

As shown in Fig. 5, if the trajectory of a satellite with some initial set of control parameters has been numerically propagated (initial trajectory), the de-orbit location of a new trajectory corresponding to the same initial conditions but a different set of control parameters can be analytically estimated by dividing the trajectories into phases where the  $C_b$  is not changing in either trajectory. In each trajectory, the phases are demarcated by the ballistic coefficient swap point ( $t_{swap}$ ), the point at which the semi major axis (orbit energy level) is the same as at the swap point of the other trajectory ( $t_{eq}$ ), and the terminal point ( $t_{term}$ ). Note that in Fig. 5, the subscript “old” refers to a parameter in the initial numerically propagated trajectory, and the subscript “new” refers to a parameter in the new trajectory that one wishes to analyze without numerically propagating. In phase 4 (below the terminal point) both trajectories have the same  $C_b$  so they can be assumed to experience the same change in orbital elements between the terminal point and the de-orbit point. For the three phases before the terminal point, Eqs. (3)–(5) can be utilized to calculate the changes in time and orbital elements experienced in each phase of the new trajectory. All changes in time and orbital elements can be added to calculate the final time and orbital elements, and hence the latitude and longitude, at the de-orbit point.

Additionally, a closed form analytical solution is derived in Ref. [16] to compute the control parameters ( $C_{b1}$ ,  $C_{b2}$ , and  $t_{swap}$ ) needed to achieve a desired total time ( $\Delta t_t$ ) and total change in argument of latitude ( $\Delta u_t$ ) to the terminal point based on  $C_{b10}$ ,  $C_{b20}$ ,  $\Delta t_{10}$ ,  $\Delta t_{20}$ ,  $\Delta u_{10}$ , and  $\Delta u_{20}$  from an original numerically propagated trajectory. These relations are

$$C_{b2} = \frac{C_{b20}(\Delta t_{20} \Delta u_{10} - \Delta t_{10} \Delta u_{20})}{\Delta t_t \Delta u_{10} - \Delta t_{10} \Delta u_t} \quad (6)$$

$$C_{b1} = \frac{\Delta u_{10} C_{b10} C_{b2}}{\Delta u_t C_{b2} - \Delta u_{20} C_{b20}} \quad (7)$$

$$t_{S_{new}} = \frac{t_{S_{old}} C_{b10}}{C_{b1}} \quad (8)$$

Note that  $C_{b10}$ ,  $\Delta t_{10}$ , and  $\Delta u_{10}$  are the ballistic coefficient, time change, and argument of latitude change between the initial time and the swap point in the initial numerically propagated trajectory and  $C_{b20}$ ,  $\Delta t_{20}$ , and  $\Delta u_{20}$  apply between the swap point and the terminal point. Note that the subscript “0” indicates a parameter applicable to the numerically propagated trajectory while parameters without the subscript “0” apply to the new trajectory that has not been propagated. Given a numerically propagated trajectory with some final impact longitude and latitude, the total argument of latitude and orbit lifetime required to de-orbit in the desired location can be calculated [16] as

$$\Delta u_t = \sin^{-1} \left( \frac{\sin(lat)}{\sin(i)} \right) \quad (9)$$

$$\Delta t_t = \Delta t_{t0} + \frac{\lambda_{imp} - \lambda_{des}}{\omega_e} \quad (10)$$

where  $\lambda$  is longitude and  $\omega_e$  is the rotation rate of the Earth. The  $\Delta t_t$  value can be adjusted using the method in Ref. [16] to ensure that the minimum targeting error is achieved within the range of feasible satellite ballistic coefficients. Note that with this method, the desired  $\Delta u_t$  will always be achieved, and  $\Delta t_t$  as close as possible to the desired one will be achieved.

A key recent update to the guidance generation algorithm is the drag-work-enforcement method that is merged into the shrinking horizon guidance generation approach. Due to the assumptions of a spherical Earth and constant density vs. altitude profile used in the analytical solution, there are often discrepancies between the numerical and analytical trajectory solutions, especially if the trajectories extend far into the future. To ensure sufficient controllability to target any point with latitude below the orbit inclination, maneuvering must begin almost two weeks in advance of the expected de-orbit. When this trajectory is simulated, the long propagation time causes the analytical

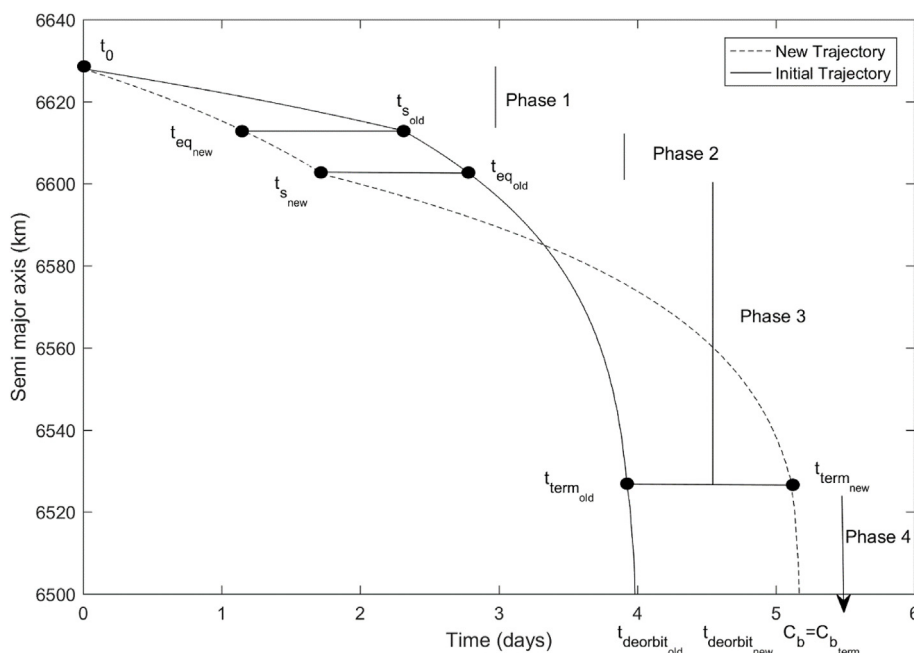


Fig. 5. Characterizing behavior of new trajectory based on old trajectory.

and numerical solutions to diverge because small errors due to the analytical solution assumptions grow over time. Conversely, if maneuvering is initiated very close to the de-orbit time (2–3 days), the analytical and numerical solutions will agree very well, but there may not be sufficient controllability to target any point on the Earth's surface. In the shrinking horizon approach (Fig. 6), when the trajectory is propagated to the de-orbit point with the ballistic coefficient profile dictated by the analytical solution, the first  $t_g$  seconds of this trajectory are stored as a part of the guidance and the trajectory after  $t_g$  is utilized to compute another analytical ballistic coefficient profile that will be numerically propagated and will be approximately  $t_g$  seconds shorter than the previously propagated trajectory. This process continues until a certain error threshold is reached or a trajectory is propagated that has less than a certain amount of orbit lifetime remaining. In the drag-work enforcement method, the work done by aerodynamic drag is recorded during the trajectory propagation, and the ballistic coefficient of the satellite during the first  $t_g$  seconds of propagation is varied so that the total work done by drag at  $t_g$  is equal to the work that should have been done by this time according to the analytical solution. In the trajectory propagation, the power or rate of change of work done by drag per unit mass can be calculated as

$$P = \dot{W}_d = -C_b \rho v_\infty (\mathbf{v}_\infty \cdot \mathbf{v}) \quad (11)$$

This expression is equivalent to the drag force (per unit mass) multiplied by the distance over which the drag is acting, divided by the time over which that distance is acted through which is the definition of power. Work done by drag is considered as a seventh state variable (in addition to the ECI position and velocity vectors) and is numerically integrated along with the position and velocity by computing  $\dot{W}_d$  using Eq. (11) at each time step. Given a numerically propagated trajectory with some  $C_b$  and  $W_d$  available at each time step, the work that should be done by drag for a trajectory with the same initial conditions but a different  $C_b$  can be calculated at some time  $t$  as follows.

1. Eq. (1) is used to calculate the time ( $t_{eq}$ ) at which the old trajectory has the same orbital energy (same semi-major axis) as the new trajectory at time  $t$ . If the ballistic coefficient is unchanging in both trajectories, this is computed by

$$t_{eq} = \frac{C_{b_{new}} t}{C_{b_0}} \quad (12)$$

2. The new trajectory should have the same  $W_d$  at  $t$  as the old, numerically propagated trajectory did at  $t_{eq}$ .

By scaling the  $C_b$  during each propagation phase to force the actual  $W_d$  to equal the analytically expected  $W_d$ , the numerically propagated trajectory is made to behave more like the analytically predicted trajectory, and thus the errors between the analytical and numerical trajectories are reduced.

Another factor that was instrumental in the reduction of guidance errors was the use of density values that were continuous in time. The NRLMSISE-00 model that was used in the orbit simulation requires current, past, and predicted F10.7 and Ap solar and geomagnetic index data. This data is reported at discrete 3-h intervals, but using such discrete, discontinuous index values leads to a density profile that is discontinuous in time. Instead, by using a cubic spline to interpolate between the F10.7 and Ap values, a set of indices, and hence a set of densities, that are continuous in time can be obtained. Because the analytical solution assumes a continuous density model, numerically propagating trajectories with a continuous density over time reduces the discrepancy between the analytical and numerical solutions and improves algorithm performance.

Ultimately, the drag-work enforcement method coupled with a continuous-time density model and the shrinking horizon guidance generation procedure causes targeting simulations run using the high fidelity NRLMSISE-00 model to experience the same high convergence rates as simulations run using the 1976 standard atmosphere.

### 3.2. Guidance tracking algorithm

The guidance tracking algorithm is detailed in Ref. [16] and a brief description is given here. The tracking algorithm involves first computing the position and velocity of the satellite relative to the guidance in the Local-Vertical-Local-Horizontal (LVLH) frame. The LVLH frame is a non-inertial reference frame defined with x-axis aligned with the zenith vector, z-axis aligned with the orbit angular momentum vector, and y-axis completing a right-handed coordinate system as shown in Fig. 7.

Let the position of the spacecraft relative to the guidance be denoted by

$$\mathbf{r}_{rel} = \mathbf{r}_{sc} - \mathbf{r}_{guid} = \begin{bmatrix} \delta x \\ \delta y \\ \delta z \end{bmatrix} \quad (13)$$

The Schweighart Sedwick (SS) dynamics [19] given by Eq. (14) provide a linearized model describing the evolution of the in-plane position and velocity of the satellite relative to the guidance in the LVLH frame based on the difference in ballistic coefficient between the

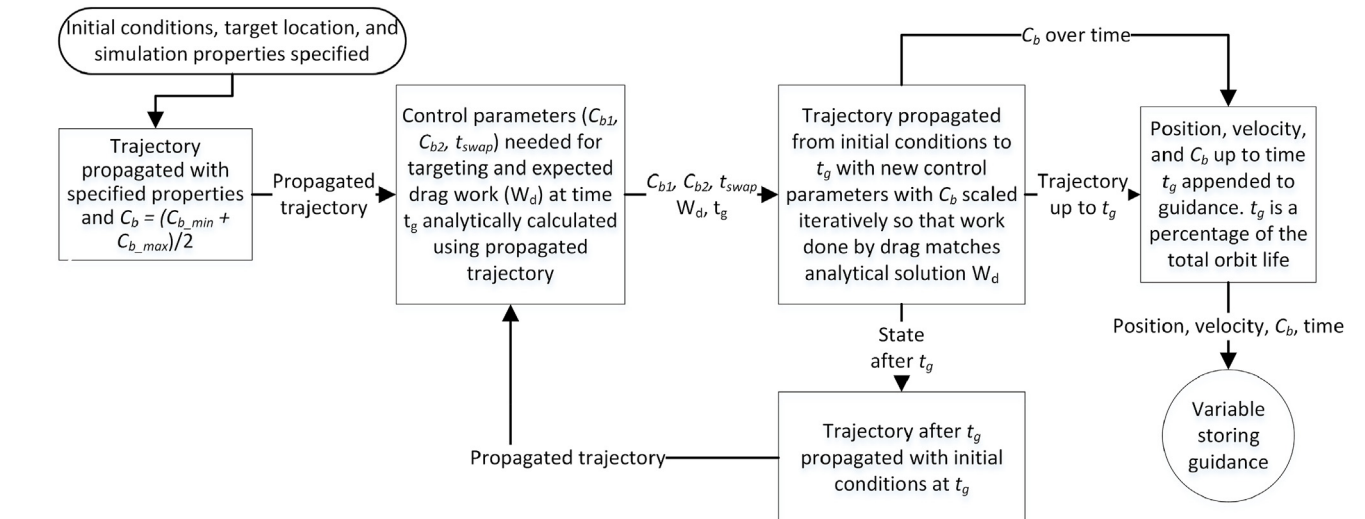


Fig. 6. Guidance generation algorithm flowchart.

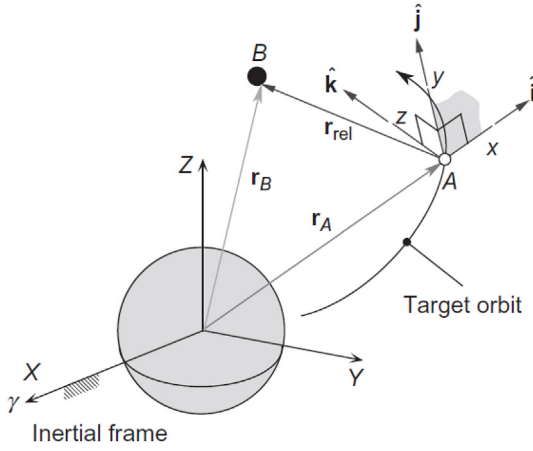


Fig. 7. LVLH Reference frame.

guidance and the actual satellite.

$$\begin{bmatrix} \delta\dot{x} \\ \delta\dot{y} \\ \delta\ddot{x} \\ \delta\dot{y} \end{bmatrix} = \begin{bmatrix} 0 & 0 & 1 & 0 \\ 0 & 0 & 0 & 1 \\ b & 0 & 0 & d \\ 0 & 0 & -d & 0 \end{bmatrix} \begin{bmatrix} \delta x \\ \delta y \\ \delta\dot{x} \\ \delta\dot{y} \end{bmatrix} + \begin{bmatrix} 0 \\ 0 \\ 0 \\ -\rho v^2 \end{bmatrix} (C_{b_{sc}} - C_{b_{guid}})$$

$$d = 2nc, \quad b = (5c^2 - 2)n^2,$$

$$c = \sqrt{1 + \frac{3J_2 R_E^2}{8a^2} [1 + 3\cos(2i)]}, \quad n = \sqrt{\frac{\mu}{a^3}} \quad (14)$$

Treating  $\Delta C_b = (C_{b_{sc}} - C_{b_{guid}})$  as a control parameter, the linear-quadratic-regulator (LQR) [20] control approach can be utilized to compute a feedback control gain ( $K$ ) that when made negative and multiplied by the relative in-plane state vector ( $x = [\delta x \ \delta y \ \delta\dot{x} \ \delta\dot{y}]^T$ ), results in a  $\Delta C_b$  that the satellite should command to drive the relative state error to zero and return to the guidance. The commanded spacecraft ballistic coefficient is thus given by

$$C_{b_{sc}} = C_{b_{guid}} - Kx \quad (15)$$

The LQR gain is computed by the MATLAB command  $K = lqr(A, B, Q, R, 0)$  where  $A$  and  $B$  are the state space dynamics matrices given in Eq. (14) and  $Q$  and  $R$  are weighting matrices on penalizing state errors and control effort respectively.  $Q$  is set to  $\begin{bmatrix} 0 & 0 & 0 & 0 \\ 0 & 1 & 0 & 0 \\ 0 & 0 & 0 & 0 \\ 0 & 0 & 0 & 0 \end{bmatrix}$  to emphasise only along-track control, and  $R$  will be a scalar that will increase if the user wants the control system to be less

aggressive and use less actuator effort.

### 3.3. Kalman filtering navigation algorithm

The details of the Kalman filtering algorithm are also given in Ref. [16], but a brief summary will be presented here. Because the LQR controller needs an estimate of the relative, not absolute, position and velocity, the LVLH position and velocity relative to the guidance can be computed for each GPS measurement and treated as the “measurement” for the purpose of the Kalman filter. A standard Extended Kalman Filter (EKF) [21] formulation is used to remove noise from this measurement. First, an initial relative state estimate ( $x_{i-1}^+$ ) is converted to the ECI frame, propagated to the time of the next available measurement and converted back to a relative position and velocity ( $x_i^-$ ). Let this numerical propagation process be denoted by  $x_i^- = f(t_i, t_{i-1}, x_{i-1}^+)$ . The estimation error covariance ( $P$ ) is then updated using the state transition matrix ( $\Phi$ ) derived from the SS dynamics as

$$\Phi_i = e^{(A-BK)(t_i-t_{i-1})} \quad (16)$$

Such that

$$x_i \approx \Phi_i x_{i-1} \quad (17)$$

This is the predict phase and can be described mathematically as

$$x_i^- = f(t_i, t_{i-1}, x_{i-1}^+)$$

$$P_i^- = \Phi_i P_{i-1}^+ \Phi_i^T + Q \quad (18)$$

where  $Q$  is a user-defined process noise covariance matrix. The actual (noisy) GPS measurement is converted to a relative in-plane position and velocity ( $z$ ) and is finally used to update the state and error covariance matrices as shown in Eq. (19).

$$S = GP_i^- G^T + W$$

$$K_i = P_i^- G^T (S)^{-1}$$

$$x_i^+ = x_i^- + K_i (z_i - Gx_i^-)$$

$$P_i^+ = (I - K_i G) P_i^- \quad (19)$$

where  $G = I_{4 \times 4}$  is the mapping from the state that is being estimated to the measurement ( $z_i = Gx_i$ ),  $W$  is a user defined measurement noise covariance matrix,  $K_i$  is the Kalman gain, and  $S$  is an intermediate term used in the calculations.  $\Lambda$  is an “anti-smugness” term set slightly greater than 1 to ensure that the process noise covariance ( $P$ ) does not become too small and lead to a lack of responsiveness of the filter to new inputs.

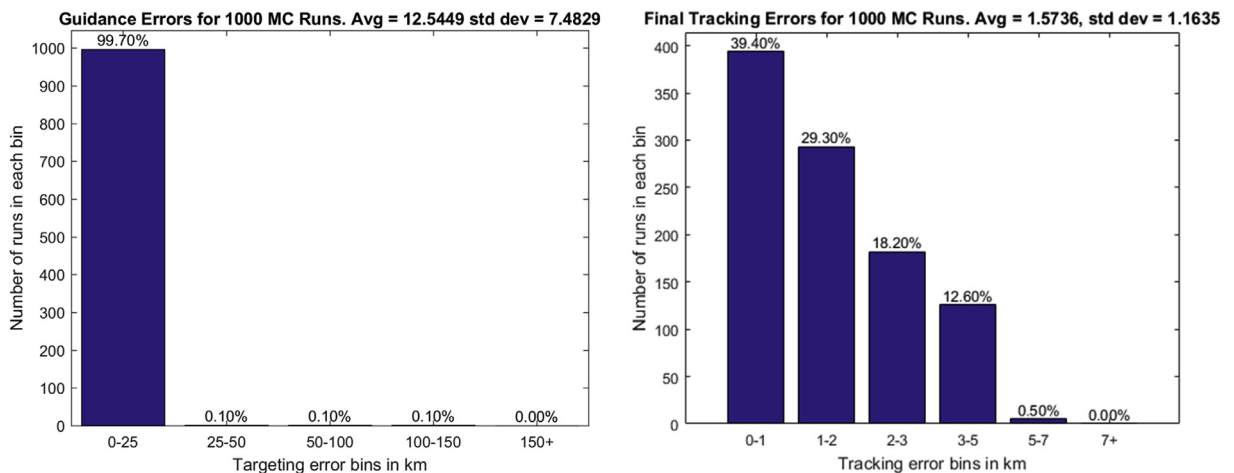


Fig. 8. Monte Carlo guidance and tracking errors.

### 3.4. Testing method

The targeting algorithm was tested using a Monte Carlo simulation approach with randomized initial condition and realistic models of drag uncertainty [22] and GPS sensor noise [23]. One thousand Monte Carlo simulations were conducted and in all cases, a guidance was generated that was trackable in a realistic environment. The average guidance error was 12.5 km with a standard deviation of 7.5 km and the average tracking error was 1.6 km down to a geodetic altitude of 120 km. 997 of the 1,000 Monte Carlo guidance simulations had a final error under 25 km which is the point where the algorithm stops seeking an improved solution. All guidance errors were below 106 km and all final tracking errors were below 7 km. Fig. 8 shows the results of the Monte Carlo guidance and tracking simulations and Fig. 9 shows the ballistic coefficient profile associated with one of the simulation runs. This simulation included sinusoidally varying density errors with periods of 26 days, 1 day, and 5400 s. As Fig. 9 shows, the tracker was able to effectively compensate for these errors. The D3 actuator was required to run for an average of 4.1% of the orbit lifetime based on the Monte Carlo simulations.

## 4. CubeSat design

The D3 satellite is designed to test the D3 device and de-orbit point targeting algorithm. Secondary objectives will include the tests of other orbital maneuvering algorithms and collision avoidance algorithms. As such, to maximize the chance of mission success, the 2U CubeSat will be built using TRL 9 parts (those with space legacy) whenever possible.

### 4.1. D3 mechanical interface

The D3 device was designed to interface easily with existing CubeSat structures. Using four M2.5 screws, an adapter stage connected to the D3 device is attached to existing holes in a standard ClydeSpace 1U structure. This serves to integrate the D3 into the structure and expand the satellite to fit the 2U form factor. The adapter also houses magnetorquers, the remove before flight pin, and the USB input port.

### 4.2. D3 electrical interface

The D3 board is the sole electrical interface between the D3 device and the rest of the CubeSat. The D3 device is connected to the D3 board via a 24-pin ribbon connector after both the D3 device and board are mechanically integrated. The magnetorquers are connected to the D3 board via a separate 6-pin ribbon cable. The D3 board is interfaced with

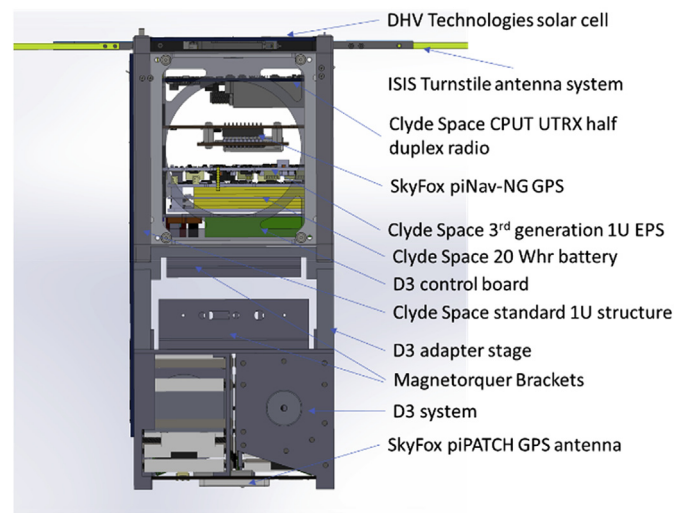


Fig. 10. Complete CubeSat structure with integrated avionics (no side solar panels).

the top of the PC104 stack (side closest to the D3) using standard PC104 pin headers as shown in Fig. 10. All avionics boards (battery, EPS, GPS, radio) are electrically connected via PC104 headers and care has been taken in selecting the configurations of the COTS boards to ensure that there are no conflicts between the PC104 pins. Fig. 11 shows the pinout of the D3 board and also indicates the signals that the D3 board will need to receive from and send to the other avionics boards. Fig. 11 also verifies that there are no conflicts between the input/output pins of the various avionics boards.

### 4.3. CubeSat structure, deployables, and solar panels

To maximize the chance of mission success, the CubeSat will be built around a standard 1U structure with significant space legacy designed and manufactured by Clyde Space. This 1U structure (Fig. 12) is designed with upper mounting holes which the manufacturer sometimes uses to convert it to a 1.5U structure. A custom-made adapter stage shown in Fig. 13 will be attached to these mounting holes and the D3 device will attach to the top of the adapter stage.

All satellite avionics will be contained in the 1U structure. The adapter stage can be manufactured using the machines at the University of Florida ADAMUS lab and in addition to connecting the D3 to the standard 1U structure, ensures that the entire CubeSat is 225 mm long

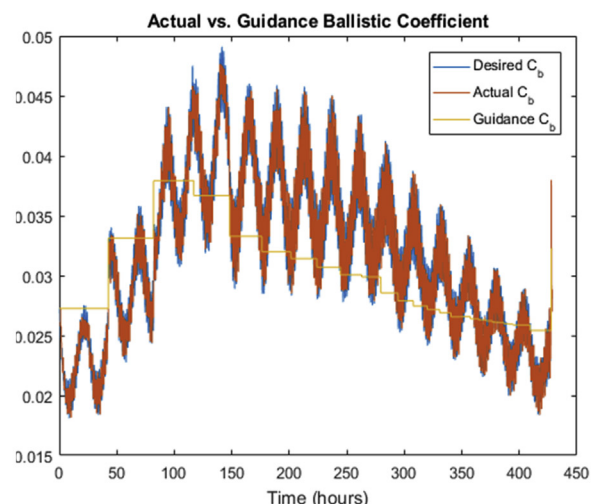
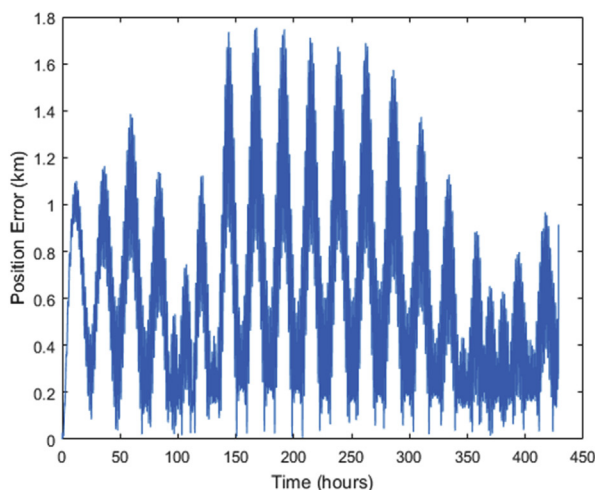


Fig. 9. Position error and ballistic coefficient over time for simulation with density uncertainty.



2	4	6	8	10	12	14	16	18	20	22	24	26	28	30	32	34	36	38	40	42	44	46	48	50	52	H2
1	3	5	7	9	11	13	15	17	19	21	23	25	27	29	31	33	35	37	39	41	43	45	47	49	51	
2	4	6	8	10	12	14	16	18	20	22	24	26	28	30	32	34	36	38	40	42	44	46	48	50	52	H1
1	3	5	7	9	11	13	15	17	19	21	23	25	27	29	31	33	35	37	39	41	43	45	47	49	51	


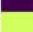

Key	
	USB Charge (H1-32)
	I2C Data (H1-41)
	I2C Clock (H1-43)
	Ground (H2-(9, 14, 17, 29, 30, 32, 47, 48))
	5V Regulated Power (H2-25, H2-26)
	3.3V Regulated Power (H2-27, H2-28)
	GPS Serial data receiver pin (H1-7)
	GPS Power on Signal (H2-50)
	GPS Timing Pin (H1-34)
	GPS Position Fix Indicator (H1-37)
	Transmit Empty (H1-1)
	Transmit Ready (H1-5)
	Receive Ready (H1-6)
	Radio Reset (H1-2)
	Independent DTMF Pins (H2-(49,51,52), H1-50)

Fig. 11. D3 board PC104 pin header configuration.

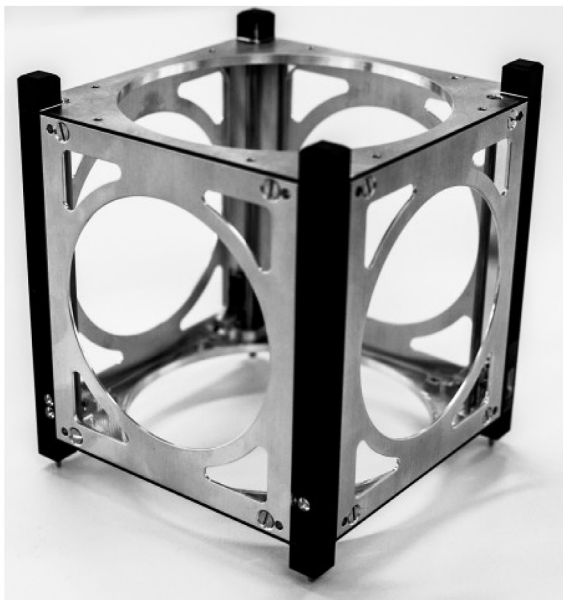


Fig. 12. Clyde space standard 1U structure.

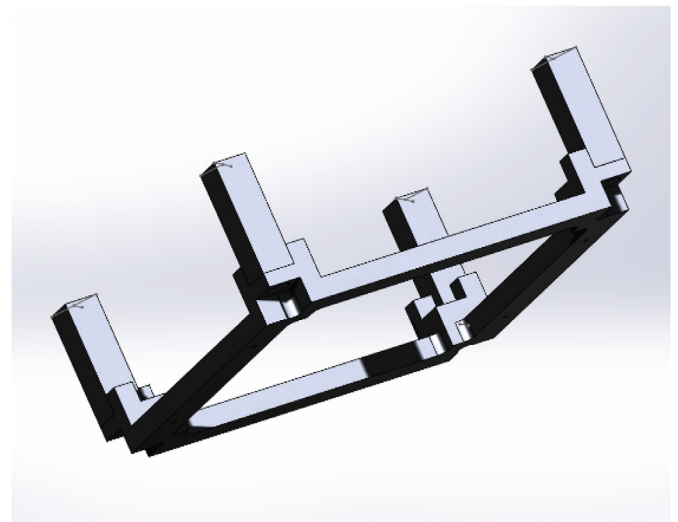


Fig. 13. D3 adapter CAD model.

Fig. 14. Fig. 16 shows a hardware prototype of the D3 mounted on a Clyde Space 1U structure to make up a cumulative 2U form factor.

as required by the design standard [24]. The adapter vertical posts are manufactured separately from the bottom plate that attaches to the 1U structure. Prior to attachment to the 1U structure, four screws are utilized to connect the adapter base, through the adapter posts, to the D3 baseplate. The placement of the adapter over the 1U structure prevents these screws from falling out of place. The complete satellite assembly when the 1U structure, adapter stage, and D3 are connected is shown in Fig. 14 and Fig. 15. A SkyFox piPATCH-L1 GPS antenna is located on top of the D3 deployer assembly which is designed to support this device. The 2U faces of the satellite will contain solar panels custom made by DHV technologies to provide room for the D3 booms to deploy. One of the panels will have holes for the remove-before-flight pin and USB charging and data cables. These panels will be fastened via M2.5 screws to the standard solar panel mounting holes built into the 1U structure. The solar panels and their locations on the D3 CubeSat are shown in

#### 4.4. Avionics

Commercially available TRL 9 avionics are used in this satellite with the exception of the D3 control board that is custom-made. All avionics are integrated into the 1U structure which supports standard PC104-sized CubeSat boards.

The COTS (commercial off the shelf) avionics include the CPUT UTRX UHF half duplex radio board sold by Clyde Space, the piNAV-NG GPS receiver made by SkyFox labs, and 20 Whr Battery and Electrical Power System boards from Clyde Space. The masses, costs, and expected power consumptions of these boards are shown in Table 1. With a maximum power output of 24 W, the EPS will be capable of running the D3 device, all avionics, and the radio simultaneously. The piNAV-NG is the lowest power commercially available CubeSat GPS, and based on the Monte Carlo simulations discussed previously, will provide

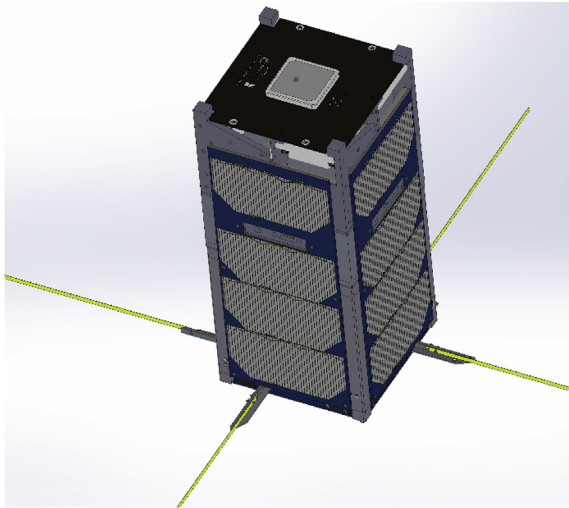


Fig. 14. D3 CubeSat with solar panels.

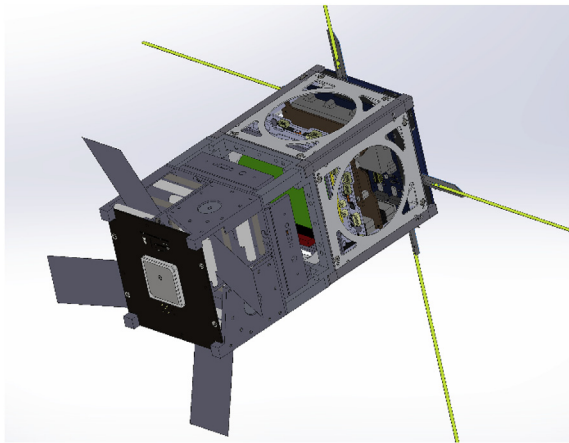


Fig. 15. D3 CubeSat without side solar panels.

sufficient accuracy for the targeting algorithms. Note that all simulations were conducted with simulated measurement noise corresponding to the manufacturer specified values for the piNAV-NG. The CPUT UTRX radio provides half duplex communication at 9600 bit/s on the 435 Mhz UHF band. The half duplex mode requires a single antenna on the ground and on the satellite for both reception and transmission. By connecting the UTRX to the ISIS turnstile antenna, an omnidirectional radiation pattern will be achieved whereby the satellite will be able to maintain contact with the ground regardless of its attitude.

The D3 system will be controlled by a single board which will host a high-performance BeagleBone Black.

Industrial processor that will also serve as the primary flight computer for the satellite. The BeagleBone will be more than capable of performing autonomous, on-board guidance generation and tracking and will connect to a PC104 sized PCB via pin headers. This PCB will also contain two TI SN754410 quad half h-bridge chips to control the D3 deployer motors and three TI DRV8837 Dual Low-Voltage H-Bridge chips to control the magnetorquers. A 24-conductor ribbon cable with vacuum rated FEP insulation will be connected to the D3 board to route signals from the D3 board to the motors and encoders. Two cables will be required for each motor and four will be needed for each encoder. A 6-pin ribbon cable will be used to route signals to the magnetorquers with two wires required for each magnetorquer. A TDK ICM-20948 9-axis IMU will also be included on the board. This chip uses only 2.4 mW and provides acceleration, angular velocity, and magnetic field measurements. These can be utilized along with the magnetometers located

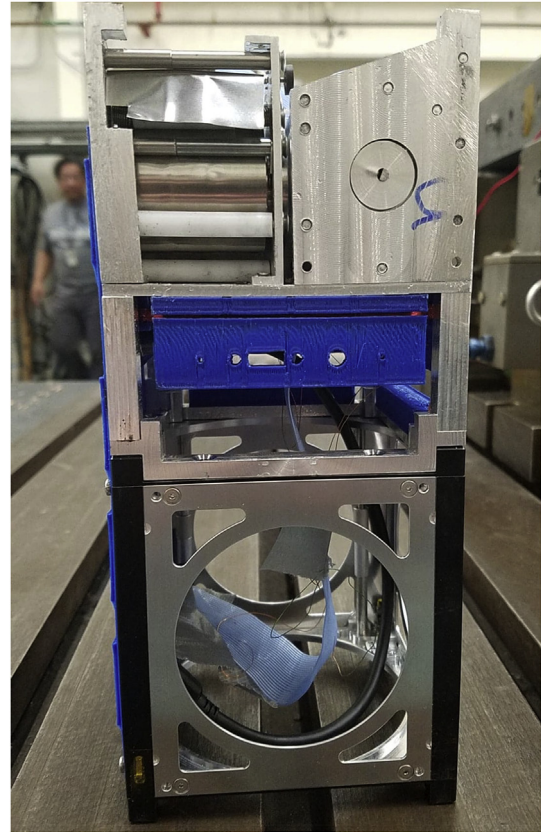


Fig. 16. CubeSat structure with D3.

on the solar panels for the B-Dot de-tumble algorithm. The D3 board will interface with the battery, EPS, GPS, and radio using the PC104 headers. Fig. 11 shows the header pin configuration for the D3 board based on the interfacing requirements specified by the manufacturers of the other avionics.

#### 4.5. Mass, power, and financial budgets

Table 1 shows the mass, power, and cost of each of the aforementioned spacecraft components. These values are given by the manufacturers for COTS components and are estimated based on the current stage of the design process for custom-made parts.

### 5. Ground station

The UHF/VHF ground station operated by the Space Systems Group at the University of Florida will be utilized for this mission. The satellite will operate in the UHF frequency in a half-duplex mode and will transmit data at 9600 bits/second. The ground station has already been used for the CHOMPTT CubeSat mission and by the time the D3 launches, the station will also have been used for the SwampSat II mission. This will reduce risk and ensure that the ground station is working properly for the D3 mission. The ground station will need to be capable of sending several basic commands to the satellite including:

- Reset microcontroller
- Update software
- Update F10.7 and AP solar and geomagnetic indices for density forecasting
- Target desired de-orbit location
- Follow pre-defined guidance trajectory
- Change operation mode (normal, debug, bare-bones)
- Manual boom deployment profile

**Table 1**  
Table of CubeSat components with masses and power usages.

Component	Mass (g)	Avg Power User (mW)	Cost (USD)
Clyde Space 3rd Generation EPS	86	160	4900
Clyde Space 20 WHr Battery	256	0	2700
Clyde Space CPUT UTRX Half Duplex Radio	90	250 RX, 4000TX, 333 avg with 30 min daily TX	8850
ISISpace Turnstile Antenna System	30	0	6891
D3 Deployers	1100	200 avg (20% duty cycle), 16400 peak	2000
D3 Magnetorquers	101	Variable, max 1000 during de-tumble	100
Beaglebone Black Master CubeSat and D3 Micro-controller	24	1000	100
DHV Technologies Custom Solar Panels (four 2U side panels, one 1U top panel)	400 total	4240 max gen. for 2U panels and 2120 max. gen. for 1U panel	26000
1U Clyde Space Structure	200	0	3550
D3 Adapter Stage	200	0	200
SkyFox piNav-NG GPS Unit	100	139	9624
SkyFox piPATCH GPS Antenna	25	100	2238
<b>Totals</b>	2612	1932 average continuous use	67153

- Request telemetry
- Update BDOT and LQR controller gains

In addition to sending down acknowledgments and status indicators in response to all received ground station commands, the satellite will need to collect and send telemetry to the ground station upon request. This telemetry will include the following information at multiple points in time.

- Battery voltage
- Solar panel voltages
- Boom deployment levels
- GPS position and velocity estimates
- Magnetometer readings
- Motor and magnetorquer usage history
- Any relevant error codes
- Current guidance trajectory

## 6. Design analysis and simulations

### 6.1. Power analysis

AGI's System's Toolkit (STK) was utilized to determine the angle of the sun with respect to each face of the satellite at each point in time. For each solar panel, the produced power was calculated (Eq. (20)) in terms of the maximum achievable power ( $P_{max}$ ) and the angle  $\theta$  between the solar panel surface normal vector and the sun vector.

$$P = P_{max} \cos(\theta) \quad (20)$$

A power analysis is included for a space-station orbit (400 km circular at 51.9° inclination) where the orbit angular momentum vector is perpendicular to the sun vector as shown in Fig. 17. This orbit represents a worst case scenario for power generation because it results in the maximum exposure of the 1U CubeSat faces to the sun and the minimum exposure of the 2U faces. This results in the lowest power generation because only one of the 1U faces has a solar panel and that panel generates only half the power of the 2U panels. Note that for the 2U side panels,  $P_{max} = 4.24 \text{ W}$  and for the 1U top panel,  $P_{max} = 2.12 \text{ W}$ . The average power generation and total energy generated by each solar panel over the course of an orbit (5554 s) is shown in Table 2 and the power generation over time profile of each panel is shown in Fig. 18. Each solar panel is defined based on the spacecraft body axis (see Fig. 1) that the normal vector of that panel aligns with. For example, the -x panel normal vector is aligned opposite the spacecraft body frame x-axis. Recall that this analysis represents a worst-case scenario for power generation. When the same power analysis was conducted for a scenario where the orbit angular momentum vector was as close as possible to parallel with the sun vector (right ascension shifted by 90° for orbit in Fig. 17), the average power generation was 3.83 W. Ideally, the

deployment level of the drag device will be planned such that when it is time to begin the re-entry point targeting algorithm (about 2 weeks before de-orbit), the satellite will be in a maximum power orbit. Even if this is not possible, however, Table 1 shows that the expected orbit-averaged power consumption will remain under 2 W. Fig. 18 shows that the satellite will never be without power generation for more than an hour at any given time, so the 20 WHr battery should be sufficient for this mission and will not drain as long as the average power consumption is less than the average power generation. As a precaution however, logic will be built into the EPS and master micro-controller to reduce the electrical load if battery charge drops below 50%.

### 6.2. Link analysis

AGI's Systems Toolkit (STK) was utilized to assess the ability to communicate with the satellite from the ground station. For the purpose of a worst case analysis, an isotropic ground antenna and the worst case antenna gain of -1dBi were considered. Atmospheric refraction and light travel time effects were also taken into account in the STK calculation. In this scenario, even when the spacecraft was located at an elevation of 5° from the ground station in a 600 km circular orbit (absolute worst case communication scenario), the signal to noise ratio was 10.8 dB with 1 Watt of RF output power (3 Watt power draw) and the bit error rate was  $1 \times 10^{-6}$  using a 9600 bits/s downlink with GMSK modulation. With 2 W RF output power (5 W power draw), the signal to noise ratio was 12 dB and the bit error rate was  $2.2 \times 10^{-12}$ . With such a high link margin even in the worst case scenario, the team can be reasonably sure that it will be possible to reliably communicate with the satellite at any point where the satellite is in view of the ground station.

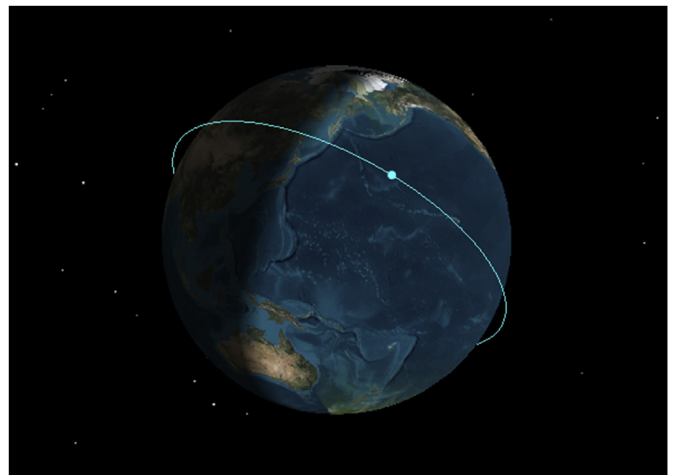


Fig. 17. Orbit with lowest power generation.

**Table 2**  
Worst case power and energy generation per orbit for each solar panel.

Panel	+x	+y	+z	-x	-y	-z	Total
Orbit-Averaged Power Generation (W)	.09	1.35	0.46	.13	0.00	.00	2.02
Energy Generated per Orbit (J)	476	7484	2532	745	0	0	11237

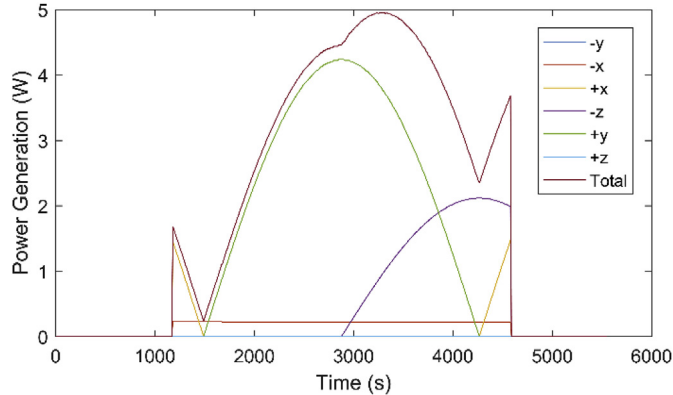


Fig. 18. Power generation by each panel over time.

6.3. Thermal analysis

The largest thermal concern in this mission is associated with the D3 device, specifically with the deployed booms. If untreated, the booms will have a solar absorptivity of 0.39 and emissivity of 0.11, resulting in maximum temperatures over 180 °C. This would be unacceptably hot and may cause thermal warping of the booms or overheating of the boom deployment electronics. To remedy this, the booms will be treated with Insta-Blak SS-370 which creates a black oxide coating and should yield an absorptivity to emissivity (A/E) ratio of close to one. This will result in boom temperatures between -94 and 68 °C which is acceptable [15]. Several boom samples made of Austenitic 316 stainless steel were treated with various concentrations of Insta-Blak and are ready for optical testing to verify the A/E ratio. Exposed aluminum elements of the D3 device will be anodized to achieve an A/E ratio of 0.8, which yields acceptable temperatures. A plot of the expected temperatures over time (after treatment) of the D3 booms and aluminum D3 shells is shown in Fig. 19.

All CubeSat avionics except the D3 board are COTS components with spaceflight legacy. Though the D3 board is made in house, the BeagleBone Black Industrial microcontroller has space flight legacy and has an operating temperature range of -40 to 85 C, so no significant thermal issues are expected. Future work will include more detailed thermal modelling and analysis of the entire spacecraft with all

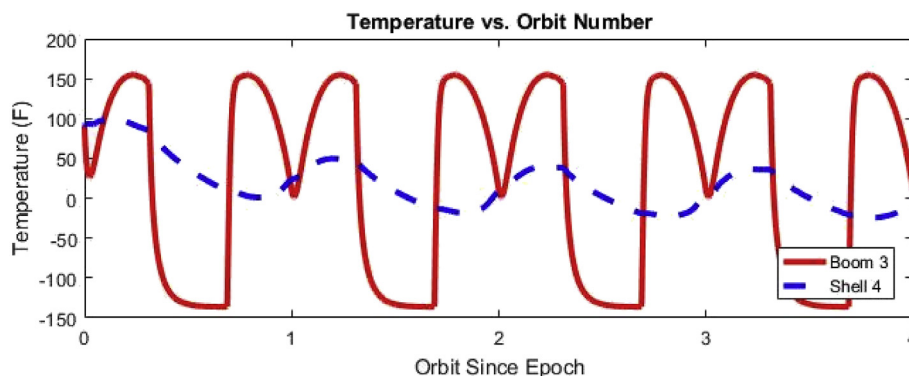


Fig. 19. D3 component temperatures over time.

components included.

6.4. Launch and structural analysis

Currently, the team plans to deploy the D3 CubeSat from the International Space Station via NanoRacks [24]. NanoRacks payloads are stored in the pressurized sections of ISS resupply vehicles, many of which are designed to carry astronauts. This means that the launch vibrational loads are quite low compared to other rideshare opportunities. However, in order to maximize the possibility of obtaining a launch, the CubeSat was designed to handle the most rigorous launch vibrational load of any vehicle currently offering CubeSat deployment. The CubeSat structure with a complete D3 device, including all four booms and magnetorquers, has been vibration tested to 9.6 GMRS in a PPOD CubeSat deployer and passed the post-vibration functional testing with no observed damage or issues.

7. Software development plan

The 2U spacecraft will host the high performance (1 GHz) BeagleBone Black processor which runs a Debian Linux operating system. Because Linux is a multi-tasking operating system, all software processes necessary to operate the spacecraft can run simultaneously without the need for multiple microcontrollers. As such, the flight software will consist of the following modules running independently on the Beaglebone using the Robot Operating System (ROS) framework:

- Command and data handling module to communicate with and route signals between all other modules
- Guidance generation module to compute trajectory that must be followed to de-orbit in desired location
- Guidance tracking module to compute D3 deployment variations necessary to track the guidance
- Attitude control module to read magnetometer data and command magnetorquers for de-tumble
- Communication module to send and receive signals from communication radio
- D3 deployer control module to actuate D3 to get desired boom deployment levels

A diagram of all relevant software modules, the connections between them, and the hardware that they interface with is shown in Fig. 20.

To ensure reliability and clarity of the code, all software modules will be written in object-oriented Python 3, with computationally intensive modules such as the guidance generation module written in C++. Test drivers will be written to verify the integrity of all module functions.

Even in low Earth orbit, high energy protons and electrons can

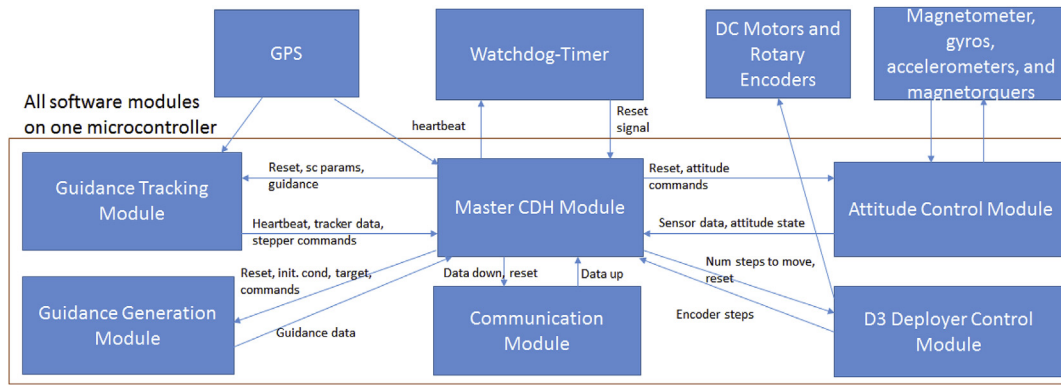


Fig. 20. Software block diagram.

cause single event upsets such as bit flips which can cause a microcontroller to operate incorrectly. Often, these upsets can be corrected by resetting the microcontroller. To perform this reset when necessary, the master command and data handling module will periodically send a pulse to one of the BeagleBone's GPIO pins that is connected to a watchdog timer. If the watchdog timer does not receive a pulse after a certain period of time, it will send a signal to reset the BeagleBone. This ensures that the BeagleBone can be reliably reset even if the processor completely locks up. Additionally, the CPU UT RX radio has digital DTMF (Dual-Tone-Multi-Frequency) pins whose voltages are set directly by the radio based on signals received from the ground. One of these pins will be tied to the reset pin on the BeagleBone so that a reset can be manually commanded even if the BeagleBone processor malfunctions in a way that does not trigger the watchdog timer.

8. Mission operations and evaluation

This section discusses the operations the satellite will undergo during the mission and the methods for assessing the success level of the mission.

8.1. Mission operations concept

The D3 mission officially begins when the CubeSat is deployed into space and the inhibit switches are released, allowing the satellite to power on. The satellite will immediately begin collecting solar power to charge its internal batteries. After the mandatory post-deployment waiting period (usually 30 min), the CubeSat will begin telemetry collection and if there is sufficient power available, will deploy the communication antennas. If there is not sufficient battery charge, the satellite will wait until there is enough power to deploy the antennas before doing anything else. After antenna deployment, the CubeSat

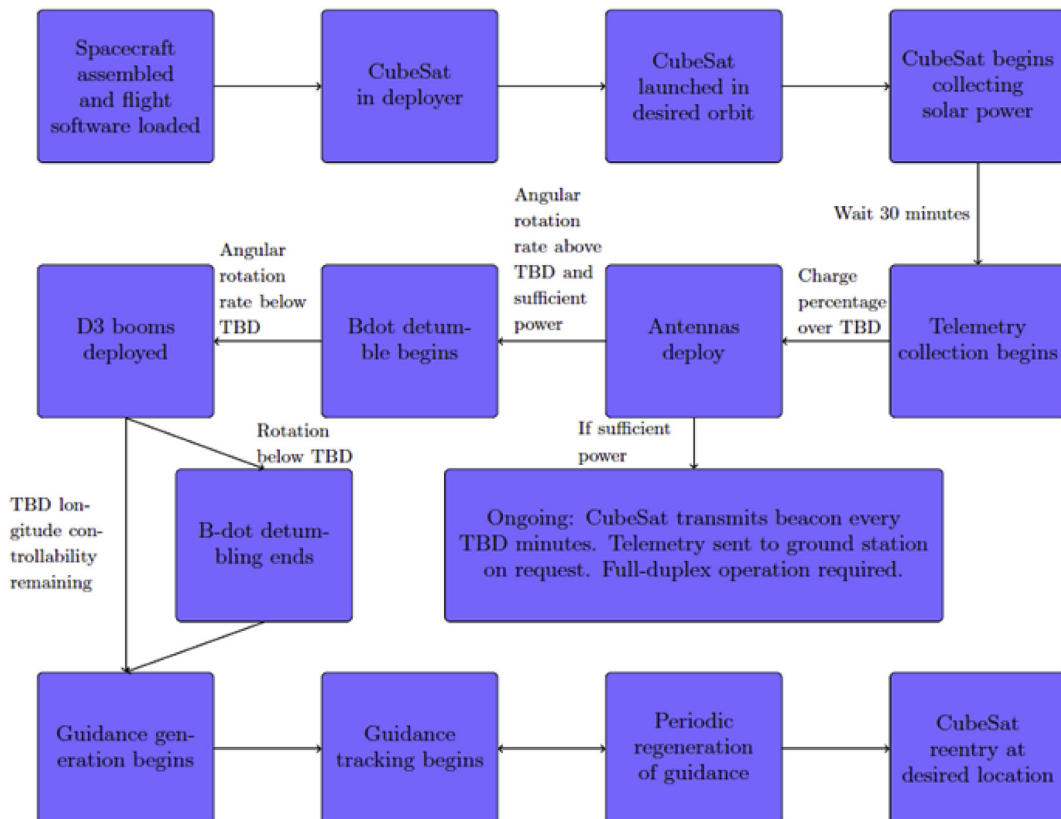


Fig. 21. D3 mission concept of operations.

begins transmitting a beacon with basic telemetry information. This beacon will help identify the location and health of the CubeSat even if communication up to the satellite is not functioning. After antenna deployment, if there is sufficient power, the CubeSat will utilize the BDot de-tumble controller to reduce its angular velocity to a certain threshold below which the booms can be safely deployed. Once the booms have been deployed and the attitude of the spacecraft has stabilized, the magnetorquers can be turned off to save power. The satellite will remain in the maximum drag configuration (booms fully deployed) until it is at a semi-major axis just high enough to provide sufficient maneuvering capabilities to target any point on the Earth with latitude below the orbit inclination. At this point, the guidance generation algorithm will be activated and will compute a drag profile and corresponding numerically propagated trajectory (guidance) that if followed, will lead the satellite to the desired re-entry location. The tracking algorithm will then be utilized to actively modulate the D3 deployment levels to ensure that the spacecraft follows this guidance despite uncertainties in the aerodynamic drag force. While the tracker is running, the guidance can be periodically updated to account for changes in the density forecasts and drifts from the initial guidance. The mission will terminate when the CubeSat re-enters the atmosphere, hopefully in the desired location. The mission phases and the conditions to go from one phase to the next are outlined in Fig. 21. The spacecraft will have on-orbit software update capabilities, so if any issues arise, ground operators can diagnose them and upload software patches. The current plan is to deploy the CubeSat from the International Space Station via NanoRacks [24], so the CubeSat is designed to conform to

the NanoRacks payload specifications. The team has applied to the CubeSat Launch Initiative (CSLI) to secure funding for a launch and deployment through NanoRacks. Because the CubeSat will be deployed from the space station, the orbit will naturally decay within a few months, even if the booms do not deploy. At the end of its life, the CubeSat will re-enter the atmosphere, and all components will burn up on re-entry, preventing the CubeSat from being a hazard to ground or space assets.

8.2. Mission success criteria

The goal of the mission is to demonstrate targeted re-entry using aerodynamic drag. However, even if this objective is not successful, other useful technology demonstrations may still be completed including demonstrations of drag device deployment and operation in space, passive attitude stabilization, and orbital maneuvering using aerodynamic drag. Fig. 22 shows the contribution to overall mission success of the partial or total fulfilment of each of these objectives. For example, if the D3 deployed and yielded the expected drag area and orbit lifetime but none of the other objectives were met, the mission would be considered 30% successful. If, the D3 deployed as expected and stabilized the spacecraft but could only track a trajectory within 110 km and the satellite failed to de-orbit in the desired location, the overall mission success level would be 60%. If all objectives were met but tracking of the CubeSat was lost at 110 km altitude and the expected position at 90 km altitude had to be estimated via simulation, the final objective in Fig. 22 would yield a 25% (instead of 30%)

D3 Capable of Modifying Drag Area (30%)	D3 maximum ballistic coefficient corresponds to expected value for full boom deployment (25%)
	D3 device de-orbits spacecraft within specified time interval (5%)
D3 device enables spacecraft to de-tumble and stabilize attitude (20%)	Spacecraft gets below 1 RPM with D3 magnetorquers only (3%)
	D3 device maintains spacecraft alignment with velocity vector within 15 degrees (13%)
	Gravity gradient stabilization within 15 degrees of nadir vector (2%) After initial stabilization, magnetorquers no longer needed (2%)
D3 device able to rendezvous with a fictitious satellite with 10 km relative position error or less (20%)	Increase success level by 1% for each 10 km that tracking error is below 210 km
D3 spacecraft de-orbits within 1300 km of a desired location at a 90 km altitude (30%)	Targeting Req. met with tracking down to 120 km altitude (-5% if not met)
	Targeting Req. met with tracking down to 90 km altitude (-5% if not met)
	Success increased by 1% for each 20 km below 1900 km error

Fig. 22. D3 mission success criteria.

**Table 3**  
Failure modes, effects, and mitigations.

Failure Mode	Potential Effect	Mitigation Strategy
Boom deployer becomes jammed or motor malfunctions	One or more booms do not deploy resulting in inaccurate drag area and attitude stability failure.	Manufacture parts to correct tolerances and with smooth surfaces to avoid jamming. Test all flight deployers. Software should detect jammed deployer and send error code. Will show up as current spike from stalled motor.
Boom does not maintain contact with rotary encoder	System will not know when to stop running deployer motor. Boom will deploy/retract until hard stop reached.	Extensively test all flight hardware. Software should detect if motor is running for extended time without encoder motion. Stronger spring roller to ensure contact with encoder.
Rotary encoder fails	System will be unable to accurately measure boom deployment level.	Can estimate deployment level from motor run time. Test hardware before flight and use best practices to mitigate ESD damage to encoder.
Screws holding D3 components together loosen during launch vibrations	Components may come apart. Loose screws may cause booms to jam or motors to lose contact with deployer drums.	Use Loctite on all screws to prevent loosening. Vibration test D3 device and complete satellite to higher vibration levels than will be expected during launch.
Single channel of encoder fails	System will think boom is either always deploying or always retracting as encoder wheel turns.	Software should be written to detect discrepancy between commanded motor direction and reported encoder direction.
Single event upset causes bit flip in BeagleBone memory	Processor locks up or gets stuck in infinite loop.	Watchdog timer in hardware and software to reset BeagleBone if periodic heartbeat is not received. Radio DTMF pins tied to BeagleBone reset to command reset directly via radio.
Software error	Can cause a variety of issues ranging from improper controller performance to communication failure to battery drain.	Ensure that software for critical communication and power management functions is working through ground testing. Software update capability to correct software problems on satellite. Hardware in the loop and day-in-the-life pre-launch testing to detect software and hardware problems.
Operating system corrupted in BeagleBone flash memory	Device may be unable to boot.	Fly with backup SD card containing OS image that BeagleBone can boot from.

contribution to the overall mission success. All other objectives would yield the maximum contribution to mission success level yielding an overall mission success of 95%. The percentages of mission success associated with each mission objective and the methods of computing the success of each objective were developed in collaboration with the initial project sponsors at the Kennedy Space Center based on what they hoped to gain from this mission.

### 8.3. Failure analysis and risk mitigation

To minimize the potential for on-orbit failures, COTS TRL9 components (those with space legacy) have been utilized wherever possible. As a result, the most probable on-orbit failures are associated with in-house components, namely the D3 device, D3 control board, and flight software. Table 3 lists potential on-orbit failures, the possible detrimental effects of each failure, and the mitigation strategy for each failure.

## 9. Conclusions

This paper presents a set of re-entry point targeting algorithms that enable a spacecraft to re-enter in a desired location solely by modulating its ballistic coefficient. Also discussed is the design of the retractable Drag De-Orbit Device (D3) and the D3 CubeSat mission which will involve a 2U, D3-equipped CubeSat that will actively modulate the D3 to autonomously control its re-entry location. The CubeSat will use commercially available TRL 9 components for the avionics, antennas, and structure with only the D3 device, structural interface adapter, and D3 control board built in-house. The D3 board, though custom-made, will use a high performance BeagleBone Black processor that has space legacy and is a TRL9 component. The use of space-tested components will increase the reliability of the satellite and the chance of mission success. After launch, the spacecraft will demonstrate the operation of the drag device, orbital maneuvering using aerodynamic drag, passive attitude stabilization using aerodynamic and gravity gradient torques, and finally, controlled re-entry using aerodynamic drag. Aerodynamically controlled re-entry methods are an efficient alternative to propulsive de-orbit burns for satellites that must de-orbit away from populated areas. These methods can be used to save fuel when de-orbiting spent launch vehicle upper stages and could also be employed for propellant-free sample return from the International Space Station. After a successful mission, the D3 device and control algorithms will

hopefully become standard tools for spacecraft attitude, orbit, and de-orbit control.

## Acknowledgements

The authors wish to thank a.i. solutions for sponsoring this investigation under a NASA Kennedy Space Center subcontract (project LSP 15–025: A Drag Device for Controlled De-Orbiting of LEO Spacecraft). This work was also supported by a NASA Space Technology Research Fellowship (Grant number 80NSSC17K0232) and funding from the Florida Space Research Initiative.

## References

- [1] W.H. Ailor, R.P. Patera, Spacecraft re-entry strategies: meeting debris mitigation and ground safety requirements, Proceedings of the Institution of Mechanical Engineers, Part G: J. Aerosp. Eng. vol 221, June 2007, pp. 947–953, <https://doi.org/10.1243/09544100JAERO199>.
- [2] NASA, “Process for Limiting Orbital Debris,” Tech. Rep. NASA-STD-8719.14A, (2012).
- [3] B. Cotton, On-orbit results from CanX-7 drag sail de-orbit mission, Proceedings of the 31st Annual AIAA/USU Conference on Small Satellites, Logan, Utah, 2017.
- [4] P. Harkness, M. McRobb, P. L’utzendorf, R. Milligan, A. Feeney, C. Clark, Development status of AEOLDOS – a deorbit module for small satellites, Adv. Space Res. 54 (2014) 82–91, <https://doi.org/10.1016/j.asr.2014.03.022>.
- [5] Re-Entry: FREEDOM Drag Sail CubeSat – Spaceflight101, (2019) Retrieved from <https://spaceflight101.com/freedom/> on January 6.
- [6] D. Guglielmo, R. Bevilacqua, Propellant-less atmospheric differential drag LEO spacecraft (PADDLES) mission, Proceedings of the 27th Annual AIAA/USU Conference on Small Satellites, Logan, UT, 2014.
- [7] M.S. Murbach, P. Papadopoulos, C. Glass, A. Dwyer-Cianciolo, R.W. Powell, S. Dutta, A. Guarneros-Luna, F.A. Tanner, A. Dono, Modeling the Exo-Brake and the Development of Strategies for De-orbit Drag Modulation, (2016).
- [8] S.S.-M. Sweil, A. Westfall, Attitude control system design for CubeSats configured with exo-brake parachute, AIAA SPACE 2016, American Institute of Aeronautics and Astronautics, 2016, <https://doi.org/10.2514/6.2016-5540>.
- [9] S. Dutta, A. Bowes, A.M. Dwyer-Cianciolo, C. Glass, R.W. Powell, Guidance scheme for modulation of drag devices to enable return from low Earth orbit, AIAA Atmospheric Flight Mechanics Conference, 2017, p. 0467, <https://doi.org/10.2514/6.2017-0467>.
- [10] D. P’erez, R. Bevilacqua, Differential drag spacecraft rendezvous using an adaptive lyapunov control strategy, Acta Astronaut. 83 (2013) 196–207, <https://doi.org/10.1016/j.actaastro.2012.09.005>.
- [11] B.S. Kumar, A. Ng, K. Yoshihara, A.D. Ruitter, Differential drag as a means of spacecraft formation control, IEEE Trans. Aerosp. Electron. Syst. 47 (2011) 1125–1135, <https://doi.org/10.1109/TAES.2011.5751247>.
- [12] C.L. Leonard, W.M. Hollister, E.V. Bergmann, Orbital formation keeping with differential drag, J. Guid. Control Dyn. 12 (1989) 108–113, <https://doi.org/10.2514/3.20374>.
- [13] L. Mazal, D. P’erez, R. Bevilacqua, F. Curti, Spacecraft rendezvous by differential

- drag under uncertainties, *J. Guid. Control Dyn.* 39 (2016) 1721–1733, <https://doi.org/10.2514/1.G001785.25>.
- [14] C. Foster, H. Hallam, J. Mason, Orbit determination and differential-drag control of planet labs cubesat constellations, *Adv. Astronaut. Sci. Astrodyn.* 156 (2015) arXiv: 1509.03270.
- [15] D. Guglielmo, S. Omar, R. Bevilacqua, L. Fineberg, J. Treptow, B. Poffenberger, Y. Johnson, Drag de-orbit device - a new standard Re-entry actuator for cubesats, *AIAA J. Spacecr. Rocket* 56 (1) (2019) 129–145. Accepted May 2018.
- [16] S. Omar, R. Bevilacqua, Guidance, navigation, and control solutions for spacecraft Re-entry point targeting using aerodynamic drag, *Acta Astronaut.* 155 (February 2019) 389–405 <https://doi.org/10.1016/j.actaastro.2018.10.016>.
- [17] J. Virgili, P. Roberts, Atmospheric interface reentry point targeting using aerodynamic drag control, *AIAA J. Guid. Control Dyn.* 38 (No. 3) (2015) 1–11, <https://doi.org/10.2514/1.G000884>.
- [18] Sanny R. Omar, Riccardo Bevilacqua, David Guglielmo, Laurence Fineberg, Justin Treptow, Scott Clark, Yusef Johnson, Spacecraft deorbit point targeting using aerodynamic drag, *J. Guid. Control Dyn.* 40 (No. 10) (2017) 2646–2652.
- [19] Samuel A. Schweighart, Raymond J. Sedwick, High-fidelity linearized J model for satellite formation flight, *J. Guid. Control Dyn.* 25 (No. 6) (2002) 1073–1080 <https://doi.org/10.2514/2.4986>.
- [20] D. Bender, A. Laub, The linear-quadratic optimal regulator for descriptor systems, *IEEE Trans. Autom. Control* 32 (8) (1987) 672–688, <https://doi.org/10.1109/TAC.1987.1104694>.
- [21] L. Ljung, Asymptotic behavior of the extended Kalman filter as a parameter estimator for linear systems, *IEEE Transactions on Automatic Control*, vol 24, 1979, pp. 36–50, , <https://doi.org/10.1109/TAC.1979.1101943> no. 1.
- [22] D.A. Vallado, D. Finkleman, A critical assessment of satellite drag and atmospheric density modeling, *Acta Astronaut.* 95 (2014) 141–165, <https://doi.org/10.1016/j.actaastro.2013.10.005>.
- [23] P. Kovář, piNAV L1—GPS receiver for small satellites, *Gyrosc. Navig.* 8 (2017) 159–164, <https://doi.org/10.1134/S2075108717020079>.
- [24] L.L.C. NanoRacks, NanoRacks CubeSat Deployer (NRCSD) Interface Control Document, (2013).